Interfacial Structure at the Quaternary Ammonium-Based Ionic Liquids|Gold Electrode Interface Probed by Surface Enhanced Infrared Absorption Spectroscopy: Anion Dependence of the Cationic Behavior

Naoya Nishi,[*,†] Kazuya Minami,[†] Kenta Motobayashi,[*,‡,¶] Masatoshi Osawa,[‡] and Tetsuo Sakka[†]

Department of Energy and Hydrocarbon Chemistry, Graduate School of Engineering, Kyoto University, Kyoto 615-8510, Japan, Institute for Catalysis, Hokkaido University, Sapporo 001-0021, Japan, and Department of Physical Science and Engineering, Graduate School of Engineering, Nagoya Institute of Technology, Nagoya 466-8555, Japan

E-mail: nishi.naoya.7e@kyoto-u.ac.jp; kmotobayashi@nitech.ac.jp

[*]To whom correspondence should be addressed
[†]Kyoto University
[‡]Hokkaido University
[¶]Nagoya Institute of Technology

Abstract

The interfacial structure at the quaternary ammonium-based ionic liquids(ILs)|gold(Au) electrode interface has been studied using surface enhanced infrared absorption spectroscopy (SEIRAS). Four anions, bis(perfluoroalkanesulfonyl)amide ($C_nC_nN^-$; $n = 0, 1, 2, 4$) have been combined with a quaternary ammonium cation, trioctylmethylammonium (N^+_{8881}), to investigate the influence of the perfluoroalkyl chain length of the anion on the behavior of the quaternary ammonium cation at the interface. In addition, to investigate the effect of the alkyl chain length of the quaternary ammonium cations on the cationic behavior, we have also combined a cation with a shorter alkyl chain, tributylmethylammonium (N^+_{4441}) with $C_1C_1N^-$. Thus, we have performed SEIRAS measurements at the Au interface of five ILs: $[N^+_{8881}][C_nC_nN^-]$ ($n = 0, 1, 2, 4$) and $[N^+_{4441}][C_1C_1N^-]$. The four CH stretching bands originating from the quaternary ammonium cations have been individually analyzed, enabling us to reveal the behavior of the quaternary ammonium cations at the interface. The cationic behavior is found to dramatically depend not only on the alkyl chain length but also on the perfluoroalkyl chain length of the counter ion. For $[N^+_{8881}][C_4C_4N^-]$ and $[N^+_{8881}][C_2C_2N^-]$, octyl chains of N^+_{8881} cannot reach the Au electrode surface at positive potentials because the bulky anions in the first ionic layer on the electrode surface block the approach. Conversely, for ILs with the smaller anions ($[N^+_{8881}][C_1C_1N^-]$ and $[N^+_{8881}][C_0C_0N^-]$) octyl chains of N^+_{8881} can penetrate into a space in the first ionic layer of small anions. The butyl chains of N^+_{4441} in $[N^+_{4441}][C_1C_1N^-]$ cannot reach the surface at positive potentials even across the first ionic layer of the small anions because of their relatively short alkyl chain length.

1 Introduction

Ionic liquids (ILs), which are entirely composed of cations and anions, have various attractive properties such as negligibly low volatility, nonflammability, electrochemical stability, and designability of various physicochemical properties.[1–3] ILs are possible candidates as

a new type of electrolyte for electrochemical devices[4–6] such as lithium ion batteries,[7–9] dye-sensitized solar cells,[10–12] electrical double layer capacitors,[13–15] and redox flow batteries.[16,17] To maximize the performance of such devices, it is of crucial importance to understand and control the structure and dynamics of ILs at the electrode interface. Several interface-selective techniques have been used to study the IL|electrode interface, such as x-ray reflectometry,[18–22] neutron reflectometry,[23,24] surface force apparatus,[25,26] atomic force microscopy,[27–30] and scanning tunneling microscopy,[31–33] in addition to theory and simulation.[3,34–44] These studies have illustrated that IL ions spontaneously form ionic multilayers[45,46] at the interface and the amount of the ions in each layer depends on the electrode potential. Such a peculiar structure at the IL interface has been found to show ultraslow dynamics[47–51] and hysteresis.[20,52–59]

Interface-selective vibrational spectroscopy techniques are powerful tools to study the IL|electrode interface. Baldelli and coworkers used sum frequency generation vibrational spectroscopy (SFG-VS) to conduct pioneering study on the interface between Pt and ILs based on 1-methyl-3-alkylimidazolium ions ($C_n$mim$^+$).[60–63] They found that the imidazolium ring of C_4mim$^+$ lies relatively parallel to the interface at negative potentials while it stand relatively perpendicular at positive potentials.[60,62,63] Other interface-selective vibrational spectroscopy techniques, infrared absorption spectroscopy (IRAS),[64] surface-enhanced infrared absorption spectroscopy (SEIRAS),[58,65] and surface-enhanced Raman spectroscopy (SERS)[66–68] have confirmed a similar trend in the orientation of the imidazolium ring. Zhou, Ouchi, and coworkers found, by using SFG-VS at the Pt interface of [C_4mim$^+$]trifluoromethane-sulfonate[55] and [C_4mim$^+$][$C_1C_1N^-$] ($C_nC_nN^-$: bis(perfluoroalkanesulfonyl)amide),[57] that the potential dependence of the vibrational bands for the IL anions exhibits hysteresis. They suggested that the hysteresis results from adsorption/desorption of the anions at the first ionic layer. Motobayashi et al. also found such a hysteresis during a potential scan in SEIRAS measurements at the Au interface of [C_4mim$^+$][$C_1C_1N^-$][58] and several other ILs.[69] Analysis of the vibrational bands for both of the IL cations and anions clarified that during

potential scans, the local ion concentration in the overlayers changes first followed by exchange of ions between the first ionic layer and the overlayers to compensate for the change in the surface charge of the electrode. The results illustrate the existence of an energy barrier for exchange of ions between the first ionic layer and the overlayers.

The electrode interface of imidazolium-based ILs has been relatively well-studied compared with other kind of ILs such as quaternary ammonium-based ILs focused in the present study. Quaternary ammonium-based ILs have an advantage over imidazolium-based ILs in that they are thermodynamically more stable against reduction, leading to a wider potential window at negative potentials.[70,71] Because of this advantage, quaternary ammonium-based ILs have been applied to electrical double layer capacitor.[13] Quaternary ammonium cations are more flexible than $C_n mim^+$ ions because they have multiple (up to four) flexible alkyl chains compared with one alkyl chain in $C_n mim^+$ ions (except methyl moiety). Such conformation flexibility would provide them interfacial structure and its potential dependence different from $C_n mim^+$ ions.

Here, we will report a SEIRAS study of the interface between Au and trialkylmethylammonium bis(perfluoroalkanesulfonyl)amide, $[N^+_{mmm1}][C_nC_nN^-]$. SEIRAS uses the enhancement of the IR electric field at the metal surface with nanometer scale roughness for its interface selectivity, and it is suitable to investigate electrical double layer (EDL) because its selectivity thickness is comparable with that of the EDL on the level of several nanometers.[72,73] In previous studies, SEIRAS has been shown to be a powerful tool to study the structure of not only the first ionic layer but also the overlayers on the Au electrode interface of imidazolium-based ILs.[58,59,69] In the present paper, we show that the structure and conformation of quaternary ammonium cations at the Au electrode interface are dramatically affected by both the alkyl chain length of the cation and the perfluoroalkyl chain length of the amide anion.

2 Experimental

2.1 Preparation of ILs

The ILs, $[N^+_{8881}][C_nC_nN^-](n = 0, 1, 2, 4)$, were prepared by mixing $[N^+_{8881}]Cl$ (Alfa Aesar) with $Li[C_0C_0N^-]$ (Nippon Shokubai), $Li[C_1C_1N^-]$ (Kanto Chemical), $H[C_2C_2N^-]$ (Central Glass) and $Li[C_4C_4N^-]$ (Mitsubishi Materials), respectively, followed by washing with water to remove the byproduct (LiCl or HCl). $[N^+_{4441}][C_1C_1N^-]$ was similarly prepared with $Li[C_1C_1N^-]$ and $[N^+_{4441}]Cl$, which was synthesized from iodomethane and tributylamine.[74] The prepared ILs were purified by column chromatography[75] and colorless liquids were obtained. The structures of some of the cations and anions used in the present study are shown in Figure 1.

2.2 SEIRAS measurements

The SEIRAS measurements were performed using the same setup as previously reported.[58,69] The working electrode was a Au film deposited on the flat surface of a semicylinder Si prism by an electroless deposition technique.[76] The counter and quasi-reference electrodes were Pt mesh and Pt wire, respectively. Before the SEIRAS experiments, the spectroelectrochemical cell filled with an IL was evacuated at 5×10^{-6} Torr at 80 °C overnight to eliminate water and other gaseous contaminants. The SEIRAS measurements were performed at 5×10^{-6} Torr and room temperature. Each SEIRA spectrum at a specific potential is a difference spectrum with respect to the spectrum at a reference potential. The reference spectrum for SEIRAS was recorded after the potential was kept at the initial potential for 200 s and just before the potential scan of cyclic voltammetry (CV). After the measurements, we checked water contents in the ILs by using the Karl Fischer titration and the contents were less than 30 ppm. Even with the low water contents, because of the enhancement effect of SEIRAS, we can detect broad O-H stretching mode of trace water in SEIRA spectra (Supporting Information). The behavior of the mode is similar to that in a recent SEIRAS study on the

IL|Au interface by Motobayashi and Osawa[59] where more intense band was observed at more positive potentials, suggesting potential-dependent accumulation of water at the interface. They found that the EDL structure and behavior in ILs are basically similar even after small amount of water (700 ppm) is intentionally added into ILs, except for slight acceleration of potential-induced structural change in the EDL.[59] Their results illustrate that the effect of water on the EDL in ILs is marginal in the level of water contents in the present study.

3 Results and discussion

3.1 ILs of large anions: $[N^+_{8881}][C_4C_4N^-]$ and $[N^+_{8881}][C_2C_2N^-]$

Figure 2a shows a CV at the $[N^+_{8881}][C_4C_4N^-]$|Au interface and Figure 2b shows typical SEIRA spectra in the CH stretching region at several electrode potentials during the positive-going potential scan of the CV, along with the IR spectrum of bulk $[N^+_{8881}][C_4C_4N^-]$ measured with the conventional attenuated total reflection (ATR) configuration without the Au film on the Si prism. In the SEIRA spectra, one can see four CH stretching vibrational bands (ν(CH)) originating from N^+_{8881} existing in the EDL at the $[N^+_{8881}][C_4C_4N^-]$|Au interface. The four bands are assigned to the symmetric and asymmetric stretching modes of the CH_2 and CH_3 moieties of N^+_{8881}. Assignment of the four bands is listed in Table 1. In the SEIRA spectra (Figure 2b), one can see a similar trend for all of the four CH stretching bands; at relatively positive (negative) potentials the bands show dips (peaks). The dips mean less absorption at the potentials than at the reference potential (−0.6 V) and can be explained from a simple electrochemical point of view; at relatively positive potentials, N^+_{8881} cations with CH_2 and CH_3 moieties are depleted in the EDL. In contrast, at relatively negative potentials, N^+_{8881} cations accumulate, resulting in peaks in the SEIRA spectra. Thus the SEIRA spectra in Figure 2b are quite reasonable when considering the local concentration of N^+_{8881} in the EDL at the electrochemical interfaces. In Fig.S1 we show SEIRA spectra in the lower wavenumber region during the same measurements exhibiting SO and CF stretching

modes, both of which originate from $C_4C_4N^-$. As expected, the potential dependence of the anion bands in Figure S1 is opposite to that of the cation bands in Figure 2; the anion bands show peaks (dips) at positive (negative) potentials, corresponding to higher (lower) local concentrations of $C_4C_4N^-$ in EDL at the $[N^+_{8881}][C_4C_4N^-]|$Au interface.

It should be noted that the behavior of the absorption bands in the SEIRA spectra is determined not only by the local concentration of the IR-active moieties in the EDL but also by their orientation. The orientation dependence of the vibration bands originates from the anisotropic direction (surface normal direction) of the IR electric field induced at the metal interface.[72,77] The absorption is proportional to the magnitude of the dot product of the transition dipole moment of the vibration bands with the IR electric field. Therefore, when the transition dipole moment is more orientated along the surface normal, the moieties interact more with the IR electric field, leading to more absorption. This mechanism, so called the surface selection rule, has been utilized to obtain information about the interfacial orientation of molecules from SEIRA spectra. The results shown in Figure 2b and Figure S1b seem to suggest that there is no drastic orientation change of both N^+_{8881} and $C_4C_4N^-$ by changing the electrode potential because the relative band intensities do not change with respect to the potential. This is opposite to the case with the electrode interface of C_4mim^+-based ILs where a drastic orientation change of the C_4mim^+ cation is observed by SEIRAS[58,65] and SFG-VS.[60] For C_4mim^+, the C_4mim^+ cation is orientated with the imidazolium ring relatively parallel to the surface at negative potentials because of the attractive electrostatic interaction between the positive charge on the imidazolium ring and the negative charge induced on the electrode surface. Conversely, at positive potentials, the electrostatic interaction changes from attractive to repulsive, leading to the C_4mim^+ orientation being relatively perpendicular to the surface. The stretching vibration of the imidazolium ring CH with a transition dipole moment parallel to the ring plane shows a stronger absorption band at positive potentials, because it interacts with the surface-normal IR electric field. The peculiarity of imidazolium ions like C_4mim^+ compared with quaternary

ammonium cations like N_{8881}^+ is probably because $C_n mim^+$ has a rigid aromatic moiety with delocalized positive charge. Such a moiety will drastically change the orientation when the surface charge on the electrode is changed. The rigid and positively charged imidazolium ring behaves differently from the flexible and neutral alkyl moieties of quaternary ammonium cations. A flexible moiety can easily change its conformation and orientation depending on its local environment and a neutral moiety is not directly affected by the surface charge on the electrode.

To more quantitatively discuss the behavior of the IR bands in Figure 2b, the intensities of the bands were evaluated by integrating the peaks. The wavenumber ranges for integration of the bands are shown in Figure 2b as the gray background and they are listed in Table 1 along with each assignment. The integration range was chosen to be sufficiently narrow to minimize the influence of overlapping neighboring bands. We did not find any Stark shift beyond the spectral resolution for the vibrational modes of the quaternary ammonium cations in the present study, although the Stark shift was reported for those of the imidazolium ring in $C_n mim^+$ ions.[66] Furthermore, the bandwidths of the bands do not vary with the electrode potential. Therefore, this way of integration is quite effective to separately focus on the potential dependence of each band. Voltabsorptograms (potential dependence of the absorption band intensity) for the four CH stretching modes during the potential scan at the $[N_{8881}^+][C_4C_4N^-]$|Au interface are shown in Figure 2c. As qualitatively observed in Figure 2b, one can see that the intensities of the cation-based bands decrease with increasing potentials. Also shown in Figure 2c is the potential of zero charge (E_{pzc}, -0.18 V, vertical dotted line), which was measured using the immersion method.[51,58,78,79] One can see that the slopes of the plots changes at E_{pzc}; a gradual slope at $E < E_{\mathrm{pzc}}$ and a steep slope at $E > E_{\mathrm{pzc}}$ for all of the bands. Because we are unsure whether this change in the slope only results from accumulation and depletion of IL ions in the EDL, not from the orientation effect, we performed a model simulation of the voltabsorptogram for IL ions in the EDL. In the model, we calculated the local concentration of IL cations and anions in the EDL and, by

combining with surface enhancement factor, we estimated the relative absorbance values of the cation and anion bands depending on the potential (details of the model are described in the Supporting Information). The model voltabsorptograms for N_{8881}^{+} and $C_4C_4N^{-}$ are shown in Figure 3. At both positive and negative potentials far away from E_{pzc}, the slope of the model voltabsorptogram for N_{8881}^{+} is gradual. The reason for the former is simple; at $E \gg E_{pzc}$ the EDL is predominantly occupied by IL anions and few IL cations remain in the EDL region (and the SEIRA enhancement region) when E becomes very positive. The latter is because of the lattice saturation,[36] that is, at sufficiently negative potentials, IL cations already occupy some of the closest ionic layers and subsequent cations coming from the bulk for charging the electrode cannot approach the electrode where SEIRA enhancement is high. The gradual slope at more negative potentials than E_{pzc} in Figure 2c is likely because of the lattice-saturation effect. The behavior of the anions in Figure S2c is similar, although there is strong hysteresis of the potential dependence of the bands. In Figure 2c and Figure S2c, one can clearly see hysteresis in the potential dependence of the band intensity. Such hysteresis has also been observed in SEIRA spectra at the Au interface of $[C_4mim^{+}][C_1C_1N^{-}]$[58] and other ILs,[69] and originates from the energy barrier for ionic exchange between the first ionic layer and the overlayers in the EDL. Hysteresis was also observed for all of the other quaternary ammonium-based ILs in the present study, indicating the generality of this phenomenon for the electrode interface of ILs (one exception has been confirmed to be $[C_4mim^{+}]BF_4^{-}$.[58,69])

To investigate the anion dependence of the ionic behaviors at the interface we performed SEIRAS measurements for $[N_{8881}^{+}][C_2C_2N^{-}]$, an IL with a smaller anion than $C_4C_4N^{-}$. $C_2C_2N^{-}$ has a shorter perfluoroalkyl moiety (perfluoroethyl) than $C_4C_4N^{-}$ (perfluorobutyl). The voltabsorptograms representing the cationic and anionic behavior are shown in Figure S4. The results are similar to those of $[N_{8881}^{+}][C_4C_4N^{-}]$, indicating that the IL anion has no influence on the interfacial structure in this ionic size range.

3.2 ILs of small anions: $[N^+_{8881}][C_1C_1N^-]$ and $[N^+_{8881}][C_0C_0N^-]$

We performed similar experiments for $[N^+_{8881}][C_1C_1N^-]$ to further diminish the anion size. Figure 4a and Figure 4b show a CV and SEIRA spectra for the $[N^+_{8881}][C_1C_1N^-]$|Au interface. The four CH stretching bands are discernible in Figure 4b, similar to Figure 2b. Their intensities vary with the potential, but the tendency is different from that in Figure 2b. The intensities of the CH_3-related bands (2875 and 2960 cm^{-1}) increase with decreasing potential, which is a similar trend to Figure 2b. However, the intensities of the CH_2-related bands (2850 and 2920 cm^{-1}) decrease in contrast to the $[N^+_{8881}][C_4C_4N^-]$ case in Figure 2b. This is also clearly seen in Figure 4c, which shows the band intensity of each band. This opposite tendency for the CH_3 and CH_2 bands indicates that the orientation effect described above surpasses the local concentration change for the $[N^+_{8881}][C_1C_1N^-]$ case as is the case with C_4mim^+.[58,60,65] It should be emphasized here that we observed such a switch of the tendency of the cation bands when we changed the IL-anion, from $C_4C_4N^-$ to $C_1C_1N^-$, illustrating that IL anions affect the interfacial behavior of IL cations. In contrast, the anion bands for $[N^+_{8881}][C_1C_1N^-]$ shown in Figure S2 exhibit a potential dependence similar to that for $[N^+_{8881}][C_4C_4N^-]$ in Figure S1. Therefore, only the N^+_{8881} cations of $[N^+_{8881}][C_1C_1N^-]$ change their orientation enough with the potential change to be observed in the SEIRA spectra.

This puzzling behavior of $[N^+_{8881}][C_1C_1N^-]$ was reproduced for $[N^+_{8881}][C_0C_0N^-]$, which is the IL of the smallest anion considered in the present study. The voltabsorptograms representing the cationic and anionic behavior are shown in Figure S5. Therefore, considering all of the data for $[N^+_{8881}][C_nC_nN^-]$, we can conclude that there must be a threshold of the anionic size to change the cationic behavior in SEIRAS from predictable to unpredictable using the simple EDL model.

Here, we consider the interfacial structure of the puzzling results for $[N^+_{8881}][C_1C_1N^-]$ and $[N^+_{8881}][C_0C_0N^-]$, that is, the ILs of the smaller anions. When $E \ll E_{pzc}$, N^+_{8881} will be preferentially located in the first ionic layer, forming a "cation layer". Because the positive charge is localized around the N atom in N^+_{8881}, the positively-charged N atom in the first ionic layer

will be attracted to the negatively-charged Au surface. Therefore, N^+_{8881} has an orientation with the methyl group pointing toward the surface and oppositely the three long octyl chains against the surface (the $[N^+_{8881}][C_1C_1N^-]$ case in Figure 6a). In such an orientation, the octyl chains are relatively directed along the surface normal, and the transition dipole moments for the two CH_2 bands are directed along the surface, leading to less interaction with the IR electric field and therefore less absorption. This view can explain why relatively low absorption of the CH_2 bands was observed at negative potentials (Figure 4c). At positive potentials, the first ionic layer is occupied by the small anions. Taking into account the increase in the CH_2 band intensity at positive potentials, the octyl chain of N^+_{8881} is likely to be inserted into the first anionic layer (Figure 6b). A recent MD simulation study of the interface between a graphene electrode and $[N^+_{2228}][C_1C_1N^-]$[43] supports this view, where the authors found that the octyl chain of N^+_{2228} in the second ionic layer is inserted into the first $C_1C_1N^-$ layer at a positive potential. Similar insertion of the octyl chains of N^+_{8881} into the first anionic layer would be the cause of the increase of the intensities of the CH_2 bands at positive potentials (Figure 4c).

Some questions remain about the potential dependent behavior of N^+_{8881}. First, why do the CH_3 bands not exhibit behavior similar to the CH_2 bands for $[N^+_{8881}][C_1C_1N^-]$ and $[N^+_{8881}][C_0C_0N^-]$? At negative potentials, the CH_3 moiety next to the N atom of N^+_{8881} will be close to the electrode surface, contributing to the high absorbance of the CH_3 bands. The other three CH_3 moieties at the terminus of the octyl chains of N^+_{8881} would make some contribution to the absorbance. At positive potentials, the small anions form the first ionic layer and the CH_3 moiety next to the N atom will not show the high absorbance because of the distance of the first anionic layer thickness from the electrode surface. Some of the octyl chains would be inserted into the first anionic layer, but not all of them. This is probably the reason why the CH_3 band behavior is predictable with the EDL model (Figure 4c). Second, how about the behavior of N^+_{8881} in $[N^+_{8881}][C_4C_4N^-]$ and $[N^+_{8881}][C_2C_2N^-]$ (ILs of the bulkier anions), after we see drastic difference for the bands of N^+_{8881} in $[N^+_{8881}][C_1C_1N^-]$ and

$[N^+_{8881}][C_0C_0N^-]$? For $[N^+_{8881}][C_4C_4N^-]$ and $[N^+_{8881}][C_2C_2N^-]$, the ILs are based on a bulkier anion than $C_1C_1N^-$ or $C_0C_0N^-$, and it would be difficult to realize such alkyl chain insertion because the bulkier anions are easily fully packed in the first ionic layer at moderate potentials (Figure 6c). Moreover, the bulkier-anion layer is thicker than the smaller-anion layer, blocking octyl chain penetration to the bottom of the first anionic layer where the surface enhancement is high. For $[N^+_{8881}][C_4C_4N^-]$ (Figure 2c) and $[N^+_{8881}][C_2C_2N^-]$ (Figure S4), the barrier formed by the bulky anionic layer would make the voltabsorptogram predictable with the EDL model (Figure 3).

3.3 IL of a short-chain cation: $[N^+_{4441}][C_1C_1N^-]$

We assumed that insertion of the octyl chains into a space in the first $C_1C_1N^-$ layer is the cause of the peculiar voltabsorptograms for $[N^+_{8881}][C_1C_1N^-]$ (Figure 4c). To examine the validity of this assumption, we adopted N^+_{4441}, quaternary ammonium cation with a shorter alkyl chain than N^+_{8881}, and studied the behavior of the cation at the Au interface of $[N^+_{4441}][C_1C_1N^-]$ by SEIRAS. We expected that the shorter chains would fail to reach the electrode surface even when they are inserted into the first $C_1C_1N^-$ layer at positive potentials, losing the peculiar behavior $[N^+_{8881}][C_1C_1N^-]$ exhibited. Figures 5b and 5c show the potential dependence of the SEIRA spectra and their band intensities of N^+_{4441} at the $[N^+_{4441}][C_1C_1N^-]|$Au interface, respectively, and Figure S5 shows anion SEIRA spectra. The potential dependence of the four CH bands reverts to simple behavior like that for $[N^+_{8881}][C_4C_4N^-]$. The butyl chains are probably inserted into the $C_1C_1N^-$ layer, however, they are too short to penetrate to the bottom of the $C_1C_1N^-$ layer (Figure 6d).

4 Conclusions

The behavior of quaternary ammonium cations at the electrode interface of quaternary ammonium-based ILs is significantly affected by the anion structure, depending on their

own alkyl chain length. This finding was made possible by utilizing SEIRAS, an interface-selective vibrational spectroscopy technique and, furthermore, by individually investigating each CH stretching vibration mode of quaternary ammonium cations.

The alkyl chains of the quaternary ammonium cations are inserted into a space in the first anionic layer. The neutral alkyl chains act as space-filling moieties, which probably have a loose structure and can be replaced by redox species coming from the IL bulk much more easily than the charged parts of IL ions forming the first ionic layer. Such replacement of the moieties of IL ions by redox species will be of crucial importance to reveal the kinetics and mechanisms of electrode reactions in ILs, especially in electrodeposition[80] and lithium-ion batteries,[44] where the redox species have to penetrate the first ionic layer and reach the interface so that they can deposit at the interface and transfer across the interface, respectively. A SEIRAS study of several quaternary ammonium-based ILs with different alkyl chain lengths containing redox species would further clarify the role of the alkyl chains.

Acknowledgement

This work was supported by JSPS KAKENHI (Nos. 25810044, 26410149, and 16H04216) and the Cooperative Research Program of the Catalysis Research Center from Hokkaido University (Nos. 12A0003 and 13A1006). The authors thank the technical division of Institute for Catalysis, Hokkaido University for their help in manufacturing the experimental equipment.

Supporting Information Available

SEIRA spectra of the anion bands ($[N^+_{8881}][C_4C_4N^-]$, $[N^+_{8881}][C_1C_1N^-]$, and $[N^+_{4441}][C_1C_1N^-]$, voltabsorptograms of the cation and anion bands for $[N^+_{8881}][C_2C_2N^-]$ and $[N^+_{8881}][C_0C_0N^-]$, details of the EDL model, and SEIRA spectra for the water stretching region.

This material is available free of charge via the Internet at `http://pubs.acs.org/`.

Table 1: Assignment of CH stretching vibration modes.

Symbol	Mode	Peak position (cm^{-1})	Integration region (cm^{-1})
$\nu_s(CH_2)$	symmetrical stretching of CH_2	2850-2866	2843-2862
$\nu_s(CH_3)^a$	symmetrical stretching of CH_3	2871-2880	2868-2881
$\nu_{as}(CH_2)$	asymmetrical stretching of CH_2	2928-2938	2914-2940
$\nu_{as}(CH_3)$	asymmetrical stretching of CH_3	2965	2953-2976

[a] Fermi resonance of $\nu_s(CH_3)$ should be around at 2915-2924 cm^{-1} but is weak and overwhelmed by the $\nu_{as}(CH_2)$ band.

Figure captions

Fig. 1 Structures of some of the ions of the ILs in the present study.

Fig. 2 (a) Cyclic voltammogram at 2 mV s^{-1} and (b) SEIRA spectra at the $[N^+_{8881}][C_4C_4N^-]||$Au interface and the IR spectrum of bulk $[N^+_{8881}][C_4C_4N^-]$. The SEIRA spectra were recorded at the potentials shown as solid circles in (a) during the CV. The reference spectrum for the SEIRAS was taken before the potential scan at the initial potential (−0.6 V). (c) Voltabsorptograms at the $[N^+_{8881}][C_4C_4N^-]||$Au interface for the four CH stretching vibrational bands: $\nu_s(CH_2)$ (solid diamonds), $\nu_s(CH_3)$ (open diamonds), $\nu_{as}(CH_2)$ (solid squares), and $\nu_{as}(CH_3)$ (open squares).

Fig. 3 Model voltabsorptogram for the electrode interface of $[N^+_{8881}][C_4C_4N^-]$.

Fig. 4 (a) Cyclic voltammogram at 2 mV s^{-1} and (b) SEIRA spectra at the $[N^+_{8881}][C_1C_1N^-]||$Au interface and the IR spectrum of bulk $[N^+_{8881}][C_1C_1N^-]$. The SEIRA spectra were recorded at the potentials shown as solid circles in (a) during the CV. The reference spectrum for the SEIRAS was taken before the potential scan at the initial potential (−0.8 V). (c) Voltabsorptograms at the $[N^+_{8881}][C_1C_1N^-]||$Au interface for the four CH stretching vibrational bands: $\nu_s(CH_2)$ (solid diamonds), $\nu_s(CH_3)$ (open diamonds), $\nu_{as}(CH_2)$ (solid squares), and $\nu_{as}(CH_3)$ (open squares).

Fig. 5 (a) Cyclic voltammogram at 2 mV s^{-1} and (b) SEIRA spectra at the $[N^+_{4441}][C_1C_1N^-]||$Au interface and the IR spectrum of bulk $[N^+_{4441}][C_1C_1N^-]$. The SEIRA spectra were recorded at the potentials shown as solid circles in (a) during the CV. The reference spectrum for the SEIRAS was taken before the potential scan at the initial potential (−0.8 V). (c) Voltabsorptograms at the $[N^+_{4441}][C_1C_1N^-]||$Au interface for the four CH stretching vibrational bands: $\nu_s(CH_2)$ (solid diamonds), $\nu_s(CH_3)$ (open diamonds), $\nu_{as}(CH_2)$ (solid squares), and $\nu_{as}(CH_3)$ (open squares).

Fig. 6 Schematics of the interfacial structures of the quaternary ammonium based ILs at the Au interface for (a,b) $[N^+_{8881}][C_1C_1N^-]$, (c) $[N^+_{8881}][C_4C_4N^-]$, and (d) $[N^+_{4441}][C_1C_1N^-]$ at (a) $E < E_{\mathrm{pzc}}$ and (b-d) $E > E_{\mathrm{pzc}}$.

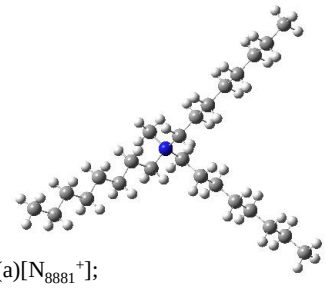

(a)[N_{8881}^{+}];
trioctylmethylammonium

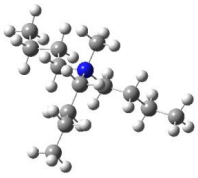

(b)[N_{4441}^{+}];
tributylmethylammonium

(c)[$C_4C_4N^{-}$];
bis(nonafluorobutanesulfonyl)amide

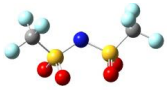

(d)[$C_1C_1N^{-}$];
bis(trifluoromethanesulfonyl)amide

Fig.1 (Nishi et al.)

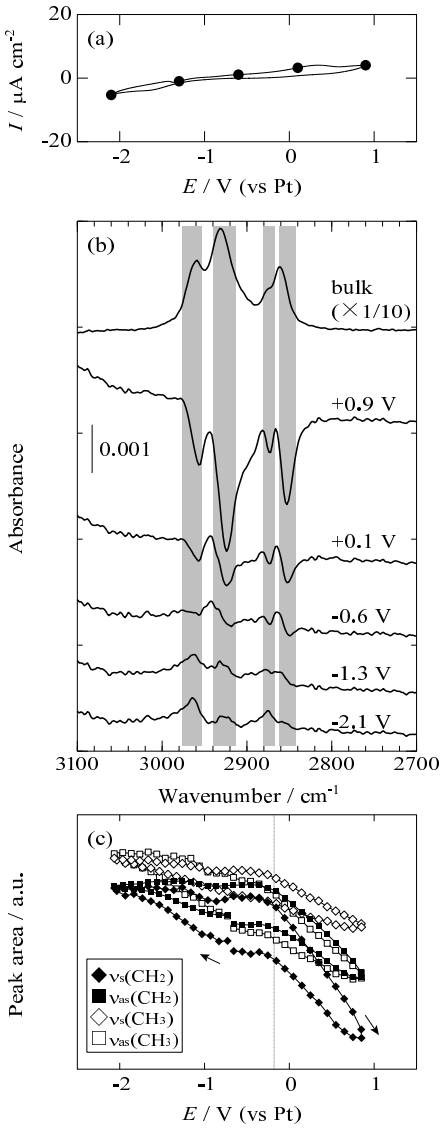

Fig.2 (Nishi et al.)

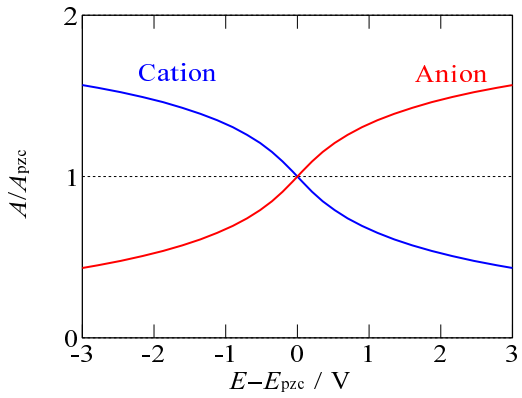

Fig.3 (Nishi et al.)

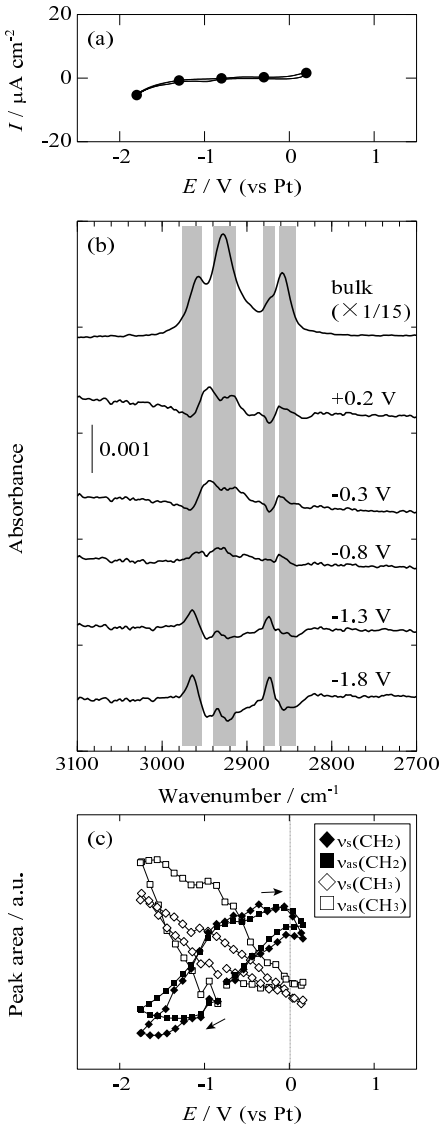

Fig.4 (Nishi et al.)

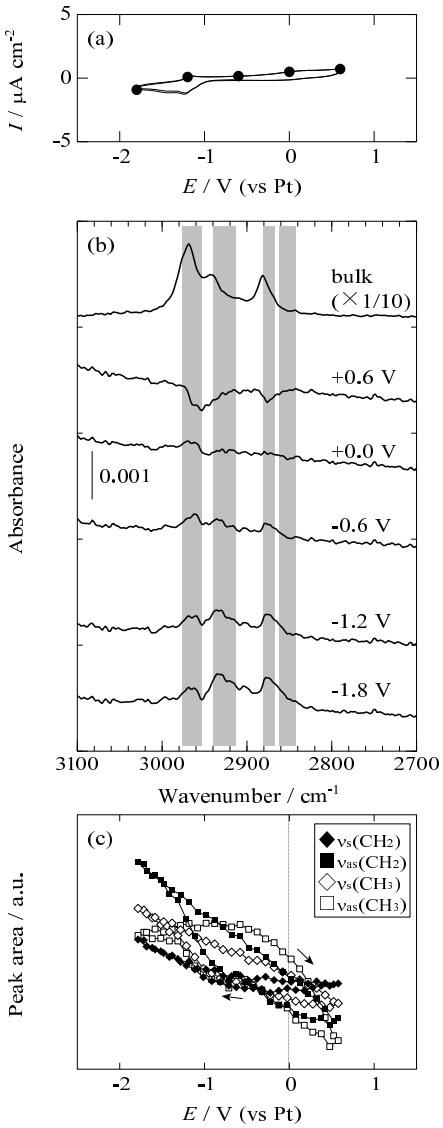

Fig.5 (Nishi et al.)

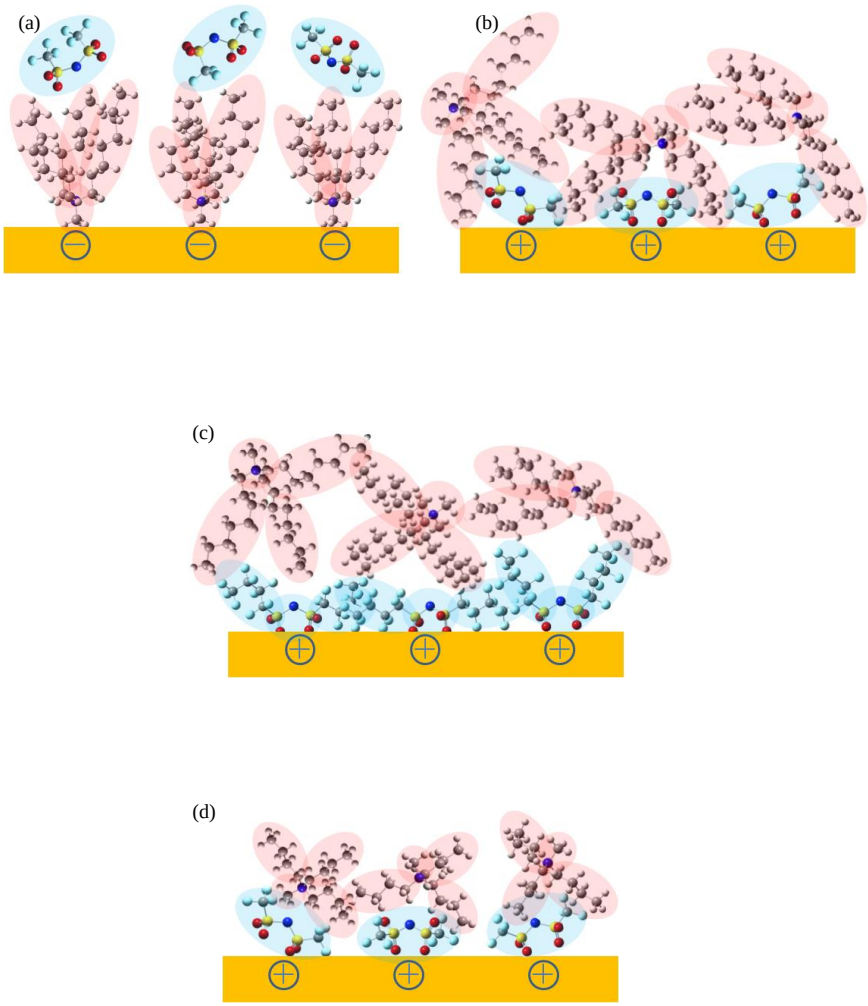

Fig.6 (Nishi et al.)

References

(1) Plechkova, N. V.; Seddon, K. R. Applications of ionic liquids in the chemical industry. *Chem. Soc. Rev.* **2008**, *37*, 123–150.

(2) Hallett, J. P.; Welton, T. Room-temperature ionic liquids: solvents for synthesis and catalysis. 2. *Chem. Rev.* **2011**, *111*, 3508–3576.

(3) Fedorov, M. V.; Kornyshev, A. A. Ionic liquids at electrified interfaces. *Chem. Rev.* **2014**, *114*, 2978–3036.

(4) Galiński, M.; Lewandowski, A.; Stępniak, I. Ionic liquids as electrolytes. *Electrochim. Acta* **2006**, *51*, 5567–5580.

(5) Armand, M.; Endres, F.; Macfarlane, D. R.; Ohno, H.; Scrosati, B. Ionic-liquid materials for the electrochemical challenges of the future. *Nat. Mater.* **2009**, *8*, 621–629.

(6) MacFarlane, D. R.; Tachikawa, N.; Forsyth, M.; Pringle, J. M.; Howlett, P. C.; Elliott, G. D.; Davis, J. H., Jr.; Watanabe, M.; Simon, P.; Angell, C. A. Energy applications of ionic liquids. *Energy Environ. Sci.* **2014**, *7*, 232–250.

(7) Nakagawa, H.; Izuchi, S.; Kuwana, K.; Nukuda, T.; Aihara, Y. Liquid and polymer gel electrolytes for lithium batteries composed of room-temperature molten salt doped by lithium salt. *J. Electrochem. Soc.* **2003**, *150*, A695–A700.

(8) Seki, S.; Kobayashi, Y.; Miyashiro, H.; Ohno, Y.; Usami, A.; Mita, Y.; Kihira, N.; Watanabe, M.; Terada, N. Lithium secondary batteries using modified-imidazolium room-temperature ionic liquid. *J. Phys. Chem. B* **2006**, *110*, 10228–10230.

(9) Wilken, S.; Xiong, S.; Scheers, J.; Jacobsson, P.; Johansson, P. Ionic liquids in lithium battery electrolytes: composition versus safety and physical properties. *J. Power Sources* **2015**, *275*, 935–942.

(10) Kubo, W.; Kitamura, T.; Hanabusa, K.; Wada, Y.; Yanagida, S. Quasi-solid-state dye-sensitized solar cells using room temperature molten salts and a low molecular weight gelator. *Chem. Commun.* **2002**, 374–375.

(11) Wang, P.; Zakeeruddin, S.; Exnar, I.; Gratzel, M. High efficiency dye-sensitized nanocrystalline solar cells based on ionic liquid polymer gel electrolyte. *Chem. Commun.* **2002**, 2972–2973.

(12) Ito, S.; Zakeeruddin, S. M.; Comte, P.; Liska, P.; Kuang, D.; Graetzel, M. Bifacial dye-sensitized solar cells based on an ionic liquid electrolyte. *Nat. Photonics* **2008**, *2*, 693–698.

(13) Sato, T.; Masuda, G.; Takagi, K. Electrochemical properties of novel ionic liquids for electric double layer capacitor applications. *Electrochim. Acta* **2004**, *49*, 3603–3611.

(14) Fechler, N.; Fellinger, T.-P.; Antonietti, M. "Salt templating": a simple and sustainable pathway toward highly porous functional carbons from ionic liquids. *Adv. Mater.* **2013**, *25*, 75–79.

(15) Brandt, A.; Pohlmann, S.; Varzi, A.; Balducci, A.; Passerini, S. Ionic liquids in supercapacitors. *MRS Bull.* **2013**, *38*, 554–559.

(16) Chakrabarti, M. H.; Mjalli, F. S.; AiNashef, I. M.; Hashim, M. A.; Hussain, M. A.; Bahadori, L.; Low, C. T. J. Prospects of applying ionic liquids and deep eutectic solvents for renewable energy storage by means of redox flow batteries. *Renew. Sust. Energ. Rev.* **2014**, *30*, 254–270.

(17) Ejigu, A.; Greatorex-Davies, P. A.; Walsh, D. A. Room temperature ionic liquid electrolytes for redox flow batteries. *Electrochem. Commun.* **2015**, *54*, 55–59.

(18) Yamamoto, R.; Morisaki, H.; Sakata, O.; Shimotani, H.; Yuan, H.; Iwasa, Y.; Kimura, T.; Wakabayashi, Y. External electric field dependence of the structure of

the electric double layer at an ionic liquid/Au interface. *Appl. Phys. Lett.* **2012**, *101*, 053122.

(19) Zhou, H.; Rouha, M.; Feng, G.; Lee, S. S.; Docherty, H.; Fenter, P.; Cummings, P. T.; Fulvio, P. F.; Dai, S.; McDonough, J. et al. Nanoscale perturbations of room temperature ionic liquid structure at charged and uncharged interfaces. *ACS Nano* **2012**, *6*, 9818–9827.

(20) Uysal, A.; Zhou, H.; Feng, G.; Lee, S. S.; Li, S.; Fenter, P.; Cummings, P. T.; Fulvio, P. F.; Dai, S.; McDonough, J. K. et al. Structural origins of potential dependent hysteresis at the electrified graphene/ionic liquid interface. *J. Phys. Chem. C* **2014**, *118*, 569–574.

(21) Uysal, A.; Zhou, H.; Feng, G.; Lee, S. S.; Li, S.; Cummings, P. T.; Fulvio, P. F.; Dai, S.; McDonough, J. K.; Gogotsi, Y. et al. Interfacial ionic 'liquids': connecting static and dynamic structures. *J. Phys.-Condes. Matter* **2015**, *27*, 032101(1–9).

(22) Chu, M.; Miller, M.; Dutta, P. Crowding and anomalous capacitance at an electrode-ionic liquid interface observed using operando x-ray scattering. *ACS Central Sci.* **2016**, *2*, 175–180.

(23) Lauw, Y.; Rodopoulos, T.; Gross, M.; Nelson, A.; Gardner, R.; Horne, M. D. Electrochemical cell for neutron reflectometry studies of the structure of ionic liquids at electrified interface. *Rev. Sci. Instrum.* **2010**, *81*, 074101.

(24) Lauw, Y.; Horne, M. D.; Rodopoulos, T.; Lockett, V.; Akgun, B.; Hamilton, W. A.; Nelson, A. R. J. Structure of $[C_4mpyr][NTf_2]$ room-temperature ionic liquid at charged gold interfaces. *Langmuir* **2012**, *28*, 7374–7381.

(25) Perkin, S. Ionic liquids in confined geometries. *Phys. Chem. Chem. Phys.* **2012**, *14*, 5052–5062.

(26) Gebbie, M. A.; Valtiner, M.; Banquy, X.; Fox, E. T.; Henderson, W. A.; Israelachvili, J. N. Ionic liquids behave as dilute electrolyte solutions. *Proc. Natl. Acad. Sci. U. S. A.* **2013**, *110*, 9674–9679.

(27) Atkin, R.; Borisenko, N.; Drüschler, M.; El Abedin, S. Z.; Endres, F.; Hayes, R.; Huber, B.; Roling, B. An in situ STM/AFM and impedance spectroscopy study of the extremely pure 1-butyl-1-methylpyrrolidinium tris(pentafluoroethyl) trifluorophosphate/Au(111) interface: potential dependent solvation layers and the herringbone reconstruction. *Phys. Chem. Chem. Phys.* **2011**, *13*, 6849–6857.

(28) Li, H.; Rutland, M. W.; Atkin, R. Ionic liquid lubrication: influence of ion structure, surface potential and sliding velocity. *Phys. Chem. Chem. Phys.* **2013**, *15*, 14616–14623.

(29) Li, H.; Endres, F.; Atkin, R. Effect of alkyl chain length and anion species on the interfacial nanostructure of ionic liquids at the Au(111)-ionic liquid interface as a function of potential. *Phys. Chem. Chem. Phys.* **2013**, *15*, 14624–14633.

(30) Harada, T.; Yokota, Y.; Imanishi, A.; Fukui, K. Preferential formation of layered structure of ionic liquid at ionic liquid aqueous solution / graphite electrode interfaces observed by frequency-modulation atomic force microscopy. *e-J. Surf. Sci. Nanotech.* **2014**, *12*, 89–96.

(31) Su, Y. Z.; Fu, Y. C.; Yan, J. W.; Chen, Z. B.; Mao, B. W. Double layer of Au(100)/ionic liquid interface and its stability in imidazolium-based ionic liquids. *Angew. Chem.-Int. Edit.* **2009**, *48*, 5148–5151.

(32) Endres, F.; Borisenko, N.; El Abedin, S. Z.; Hayes, R.; Atkin, R. The interface ionic liquid(s)/electrode(s): in situ STM and AFM measurements. *Faraday Discuss.* **2012**, *154*, 221–233.

(33) Wen, R.; Rahn, B.; Magnussen, O. M. Potential-dependent adlayer structure and dy-

namics at the ionic liquid/Au(111) interface: a molecular-scale in situ video-STM study. *Angew. Chem.-Int. Edit.* **2015**, *54*, 6062–6066.

(34) Pinilla, C.; Del Pópolo, M. G.; Kohanoff, J.; Lynden-Bell, R. M. Polarization relaxation in an ionic liquid confined between electrified walls. *J. Phys. Chem. B* **2007**, *111*, 4877–4884.

(35) Reed, S. K.; Lanning, O. J.; Madden, P. A. Electrochemical interface between an ionic liquid and a model metallic electrode. *J. Chem. Phys.* **2007**, *126*, 084704(1–13).

(36) Kornyshev, A. A. Double-layer in ionic liquids: paradigm change? *J. Phys. Chem. B* **2007**, *111*, 5545–5557.

(37) Oldham, K. B. A Gouy-Chapman-Stern model of the double layer at a (metal)/(ionic liquid) interface. *J. Electroanal. Chem.* **2008**, *613*, 131–138.

(38) Kislenko, S. A.; Samoylov, I. S.; Amirov, R. H. Molecular dynamics simulation of the electrochemical interface between a graphite surface and the ionic liquid [BMIM][PF_6]. *Phys. Chem. Chem. Phys.* **2009**, *11*, 5584–5590.

(39) Feng, G.; Zhang, J. S.; Qiao, R. Microstructure and capacitance of the electrical double layers at the interface of ionic liquids and planar electrodes. *J. Phys. Chem. C* **2009**, *113*, 4549–4559.

(40) Vatamanu, J.; Borodin, O.; Smith, G. D. Molecular insights into the potential and temperature dependences of the differential capacitance of a room-temperature ionic liquid at graphite electrodes. *J. Am. Chem. Soc.* **2010**, *132*, 14825–14833.

(41) Bazant, M. Z.; Storey, B. D.; Kornyshev, A. A. Double layer in ionic liquids: overscreening versus crowding. *Phys. Rev. Lett.* **2011**, *106*, 046102(1–4).

(42) Merlet, C.; Salanne, M.; Rotenberg, B.; Madden, P. A. Imidazolium ionic liquid interfaces with vapor and graphite: interfacial tension and capacitance from coarse-grained molecular simulations. *J. Phys. Chem. C* **2011**, *115*, 16613–16618.

(43) Sharma, S.; Kashyap, H. K. Structure of quaternary ammonium ionic liquids at interfaces: effects of cation tail modification with isoelectronic groups. *J. Phys. Chem. C* **2015**, *119*, 23955–23967.

(44) Ivanistsev, V.; Mendez-Morales, T.; Lynden-Bell, R. M.; Cabeza, O.; Gallego, L. J.; Varela, L. M.; Fedorov, M. V. Molecular origin of high free energy barriers for alkali metal ion transfer through ionic liquid-graphene electrode interfaces. *Phys. Chem. Chem. Phys.* **2016**, *18*, 1302–1310.

(45) Mezger, M.; Schröder, H.; Reichert, H.; Schramm, S.; Okasinski, J. S.; Schöder, S.; Honkimäki, V.; Deutsch, M.; Ocko, B. M.; Ralston, J. et al. Molecular layering of fluorinated ionic liquids at a charged sapphire (0001) surface. *Science* **2008**, *322*, 424–428.

(46) Nishi, N.; Yasui, Y.; Uruga, T.; Tanida, H.; Yamada, T.; Nakayama, S.; Matsuoka, H.; Kakiuchi, T. Ionic multilayers at the free surface of an ionic liquid, trioctylmethylammonium bis(nonafluorobutanesulfonyl)amide, probed by x-ray reflectivity measurements. *J. Chem. Phys.* **2010**, *132*, 164705.

(47) Yasui, Y.; Kitazumi, Y.; Ishimatsu, R.; Nishi, N.; Kakiuchi, T. Ultraslow response of interfacial tension to the change in the phase-boundary potential at the interface between water and a room-temperature ionic liquid, trioctylmethylammonium bis(nonafluorobutanesulfonyl)amide. *J. Phys. Chem. B* **2009**, *113*, 3273–3276.

(48) Bou-Malham, I.; Bureau, L. Nanoconfined ionic liquids: effect of surface charges on flow and molecular layering. *Soft Matter* **2010**, *6*, 4062–4065.

(49) Makino, S.; Kitazumi, Y.; Nishi, N.; Kakiuchi, T. Charging current probing of the slow relaxation of the ionic liquid double layer at the Pt electrode. *Electrochem. Commun.* **2011**, *13*, 1365–1368.

(50) Drüschler, M.; Borisenko, N.; Wallauer, J.; Winter, C.; Huber, B.; Endres, F.; Roling, B. New insights into the interface between a single-crystalline metal electrode and an extremely pure ionic liquid: slow interfacial processes and the influence of temperature on interfacial dynamics. *Phys. Chem. Chem. Phys.* **2012**, *14*, 5090–5099.

(51) Nishi, N.; Hirano, Y.; Motokawa, T.; Kakiuchi, T. Ultraslow relaxation of the structure at the ionic liquid|gold electrode interface to a potential step probed by electrochemical surface plasmon resonance measurements: asymmetry of the relaxation time to the potential-step direction. *Phys. Chem. Chem. Phys.* **2013**, *15*, 11615–11619.

(52) Lockett, V.; Sedev, R.; Ralston, J.; Horne, M.; Rodopoulos, T. Differential capacitance of the electrical double layer in imidazolium-based ionic liquids: influence of potential, cation size, and temperature. *J. Phys. Chem. C* **2008**, *112*, 7486–7495.

(53) Drüschler, M.; Huber, B.; Passerini, S.; Roling, B. Hysteresis effects in the potential-dependent double layer capacitance of room temperature ionic liquids at a polycrystalline platinum interface. *J. Phys. Chem. C* **2010**, *114*, 3614–3617.

(54) Gore, T. R.; Bond, T.; Zhang, W.; Scott, R. W. J.; Burgess, I. J. Hysteresis in the measurement of double-layer capacitance at the gold-ionic liquid interface. *Electrochem. Commun.* **2010**, *12*, 1340–1343.

(55) Zhou, W.; Inoue, S.; Iwahashi, T.; Kanai, K.; Seki, K.; Miyamae, T.; Kim, D.; Katayama, Y.; Ouchi, Y. Double layer structure and adsorption/desorption hysteresis of neat ionic liquid on Pt electrode surface - an in-situ IR-visible sum-frequency generation spectroscopic study. *Electrochem. Commun.* **2010**, *12*, 672–675.

(56) Alam, M. T.; Masud, J.; Islam, M. M.; Okajima, T.; Ohsaka, T. Differential capacitance at Au(111) in 1-alkyl-3-methylimidazolium tetrafluoroborate based room-temperature ionic liquids. *J. Phys. Chem. C* **2011**, *115*, 19797–19804.

(57) Zhou, W.; Xu, Y.; Ouchi, Y. Hysteresis effects in the in-situ SFG and differential capacitance measurements on metal electrode/ionic liquids interface. *ECS Trans.* **2012**, *50*, 339–348.

(58) Motobayashi, K.; Minami, K.; Nishi, N.; Sakka, T.; Osawa, M. Hysteresis of potential-dependent changes in ion density and structure of an ionic liquid on a gold electrode: in situ observation by surface-enhanced infrared absorption spectroscopy. *J. Phys. Chem. Lett.* **2013**, *4*, 3110–3114.

(59) Motobayashi, K.; Osawa, M. Potential-dependent condensation of water at the interface between ionic liquid [BMIM][TFSA] and an Au electrode. *Electrochem. Commun.* **2016**, *65*, 14–17.

(60) Rivera-Rubero, S.; Baldelli, S. Surface spectroscopy of room-temperature ionic liquids on a platinum electrode: a sum frequency generation study. *J. Phys. Chem. B* **2004**, *108*, 15133–15140.

(61) Baldelli, S. Probing electric fields at the ionic liquid-electrode interface using sum frequency generation spectroscopy and electrochemistry. *J. Phys. Chem. B* **2005**, *109*, 13049–13051.

(62) Aliaga, C.; Baldelli, S. Sum frequency generation spectroscopy and double-layer capacitance studies of the 1-butyl-3-methylimidazolium dicyanamide-platinum interface. *J. Phys. Chem. B* **2006**, *110*, 18481–18491.

(63) Baldelli, S. Surface structure at the ionic liquid-electrified metal interface. *Accounts Chem. Res.* **2008**, *41*, 421–431.

(64) Nanbu, N.; Sasaki, Y.; Kitamura, F. In situ FT-IR spectroscopic observation of a room-temperature molten salt vertical bar gold electrode interphase. *Electrochem. Commun.* **2003**, *5*, 383–387.

(65) Nanbu, N.; Kato, T.; Sasaki, Y.; Kitamura, F. In situ SEIRAS study of room-temperature ionic liquid vertical bar gold electrode interphase. *Electrochemistry* **2005**, *73*, 610–613.

(66) V. O. Santos, J.; Alves, M. B.; Carvalho, M. S.; Suarez, P. A. Z.; Rubim, J. C. Surface-enhanced raman scattering at the silver electrode/ionic liquid ($BMIPF_6$) interface. *J. Phys. Chem. B* **2006**, *110*, 20379–20385.

(67) Rubim, J. C.; Trindade, F. A.; Gelesky, M. A.; Aroca, R. F.; Dupont, J. Surface-enhanced vibrational spectroscopy of tetrafluoroborate 1-n-butyl-3-methylimidazolium ($BMIBF_4$) ionic liquid on silver surfaces. *J. Phys. Chem. C* **2008**, *112*, 19670–19675.

(68) Brandao, C. R. R.; Costa, L. A. F.; Breyer, H. S.; Rubim, J. C. Surface-enhanced raman scattering (SERS) of a copper electrode in 1-n-butyl-3-methylimidazolium tetrafluoroborate ionic liquid. *Electrochem. Commun.* **2009**, *11*, 1846–1848.

(69) Motobayashi, K.; Nishi, N.; Inoue, Y.; Minami, K.; Sakka, T.; Osawa, M. Potential-induced restructuring dynamics of ionic liquids on a gold electrode: steric effect of constituent ions studied by surface-enhanced infrared absorption spectroscopy. *J. Electroanal. Chem.* submitted.

(70) Sun, J.; Forsyth, M.; MacFarlane, D. R. Room-temperature molten salts based on the quaternary ammonium ion. *J. Phys. Chem. B* **1998**, *102*, 8858–8864.

(71) Matsumoto, H.; Yanagida, M.; Tanimoto, K.; Nomura, M.; Kitagawa, Y.; Miyazaki, Y. Highly conductive room temperature molten salts based on small trimethylalkylammonium cations and bis(trifluoromethylsulfonyl)imide. *Chem. Lett.* **2000**, 922–923.

(72) Osawa, M. Dynamic processes in electrochemical reactions studied by surface-enhanced infrared absorption spectroscopy (SEIRAS). *Bull. Chem. Soc. Jpn.* **1997**, *70*, 2861–2880.

(73) Osawa, M.; Tsushima, M.; Mogami, H.; Samjeske, G.; Yamakata, A. Structure of water at the electrified platinum-water interface: a study by surface-enhanced infrared absorption spectroscopy. *J. Phys. Chem. C* **2008**, *112*, 4248–4256.

(74) Pal, K.; Pore, S. K.; Sinha, S.; Janardhanan, R.; Mukhopadhyay, D.; Banerjee, R. Structure-activity study to develop cationic lipid-conjugated haloperidol derivatives as a new class of anticancer therapeutics. *J. Med. Chem.* **2011**, *54*, 2378–2390.

(75) Earle, M. J.; Gordon, C. M.; Plechkova, N. V.; Seddon, K. R.; Welton, T. Decolorization of ionic liquids for spectroscopy. *Anal. Chem.* **2007**, *79*, 758–764.

(76) Miyake, H.; Ye, S.; Osawa, M. Electroless deposition of gold thin films on silicon for surface-enhanced infrared spectroelectrochemistry. *Electrochem. Commun.* **2002**, *4*, 973–977.

(77) Osawa, M.; Ataka, K.; Yoshii, K.; Nishikawa, Y. Surface-enhanced infrared-spectroscopy - the origin of the absorption enhancement and band selection rule in the infrared-spectra of molecules adsorbed on fine metal particles. *Appl. Spectrosc.* **1993**, *47*, 1497–1502.

(78) Jakuszewski, B.; Kozowski, Z. Pomiar potenciału ładunku zerowego metoda zanurzeniowa. *Rocz. Chem.* **1962**, *36*, 1873–1877.

(79) Nishi, N.; Uchiyashiki, J.; Oogami, R.; Sakka, T. Ionic liquid structure at the electrified ionic liquid|Hg interface studied using in situ spectroscopic ellipsometry. *Thin Solid Films* **2014**, *571*, 735–738.

(80) Endres, F.; Hoefft, O.; Borisenko, N.; Gasparotto, L. H.; Prowald, A.; Al-Salman, R.; Carstens, T.; Atkin, R.; Bund, A.; El Abedin, S. Z. Do solvation layers of ionic liquids influence electrochemical reactions? *Phys. Chem. Chem. Phys.* **2010**, *12*, 1724–1732.

TOC Graphic

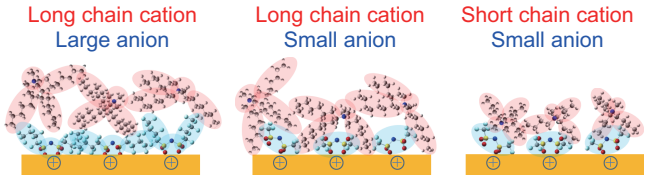
Long chain cation
Large anion
Long chain cation
Small anion
Short chain cation
Small anion